The TDDFT Excitation Energies of the BODIPYs; The DFT and TDDFT Challenge Continues

Adrien Schlachter, Alexandre Fleury, Kevin Tanner, Armand Soldera, Benoit Habermeyer, Roger Guilard, Pierre D Harvey

molecules

MDPI

Article

The TDDFT Excitation Energies of the BODIPYs; The DFT and TDDFT Challenge Continues

Adrien Schlachter [1], Alexandre Fleury [1], Kevin Tanner [1], Armand Soldera [1], Benoit Habermeyer [2,3], Roger Guilard [2,3] and Pierre D. Harvey [1,*]

[1] Département de Chimie, Université de Sherbrooke, 25000, Boul. de l'Université, Sherbrooke, QC J1K 2R1, Canada; adrien.schlachter@usherbrooke.ca (A.S.); Alexandre.Fleury@USherbrooke.ca (A.F.); kevin.tanner@usherbrooke.ca (K.T.); Armand.Soldera@USherbrooke.ca (A.S.)
[2] PorphyChem Porphyrin Chemicals & Engineering, 21000 Dijon, France; b.habermeyer@porphychem.com (B.H.); Roger.Guilard@u-bourgogne.fr (R.G.)
[3] Institut de Chimie Moléculaire de l'Université de Bourgogne, ICMUB, Université de Bourgogne Franche-Comté UMR CNRS 6302, F-21078 Dijon, France
* Correspondence: pierre.harvey@usherbrooke.ca; Tel.: +1-819-821-8000-67092

Abstract: The derivatives of 4,4-difluoro-4-bora-3a,4a-diaza-s-indacene (BODIPY) are pivotal ingredients for a large number of functional, stimuli-responsive materials and therapeutic molecules based on their photophysical properties, and there is a urgent need to understand and predict their optical traits prior to investing a large amount of resources in preparing them. Density functional theory (DFT) and time-dependent DFT (TDDFT) computations were performed to calculate the excitation energies of the lowest-energy singlet excited state of a large series of common BODIPY derivatives employing various functional aiming at the best possible combination providing the least deviations from the experimental values. Using the common "fudge" correction, a series of combinations was investigated, and a methodology is proposed offering equal or better performances than what is reported in the literature.

Keywords: BODIPY; DFT; TDFT

Citation: Schlachter, A.; Fleury, A.; Tanner, K.; Soldera, A.; Habermeyer, B.; Guilard, R.; Harvey, P.D. The TDDFT Excitation Energies of the BODIPYs; The DFT and TDDFT Challenge Continues. *Molecules* **2021**, *26*, 1780. https://doi.org/10.3390/molecules26061780

Academic Editors: Wong Wai-Yeung (Raymond) and Sakamoto Ryota

Received: 23 February 2021
Accepted: 18 March 2021
Published: 22 March 2021

1. Introduction

The BODIPY pigment and its derivatives are key entities for phototheranostics [1], including photodynamic therapy [2], functional optoelectronic materials [3], such as solar cells [4–6] and light emitting diodes [7], and stimuli-responsive materials [8–11]. In order to understand or predict the optical properties [12,13] of such important chromophore, and notably the lowest energy electronic transition, a very large number of investigations involving computational argumentations were reported but most of the time the correspondence between the calculated position and experimentally observed one turned out to be chronically poor, where differences ranging from 60 to 100 nm were commonly depicted [14–27]. However, on some rare occasions, the comparison between computations and experiments appeared much better [28,29]. In front of this curious phenomenon, multiple theoretical investigations were undertaken [30–36], and emphasis on the computational method, types of the basis sets, the importance of the solvent field, the use of excited state molecular dynamics, and even empirical corrections, were made [37–46]. Ab initio calculations were also reported with good results, but the computational time is also an unneglectable parameter to consider [47,48].

From all these previous investigations, the main conclusion is that the methodology that requires the least resources in material science and biomedical research is the application of an empirical correction: "*fudge*" [18,38,49]. Fudge methods generally consist in applying an empirical correction to calculated data to make them fit with experimental

results. Usually, this method is used for TD-DFT computations where the shape of the simulated spectra compare favorably with the experiments but exhibit large offsets in terms of wavelength position.

This work proposes a revisit where new basis sets and computational methods are applied to find the best combination in order to provide a better agreement between computations and experiments. Figure 1 depicts the structure of the BODIPY core and its classical numbering scheme, for the purpose of this paper, the alpha, beta, and meso designation will be used.

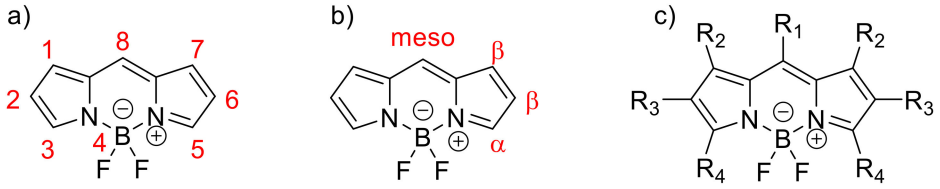

Figure 1. 4,4-difluoro-4-bora-3a,4a-diaza-s-indacene (BODIPY) core. (**a**), IUPAC (International Union of Pure and Applied Chemistry) numbering. (**b**), alpha, beta, and meso designation. (**c**), investigated structures.

2. Investigated Structures

All investigated structures and experimental parameters were selected from ref [50] and categorized into five families (Figure 1 and Table 1): hydrogen in meso and *α* and *β* substitution (**B1**–**5**), aromatic in meso and α and β substitution (**B6**–**9**), substitution on aromatic position (**B10**–**B13**), meso-amino derivatives (**B14**–**B19**), meso-*alkoxy* derivatives (**B20**–**23**) and others (**B24**–**B30**) containing BODIPYs with extended pi-systems composed by *α*-vinyl, β-conjugated and aza-BODIPYs. A test group (Table 2) is also described to verify the robustness of our model composed with 10 representative pyrrole-based dyes (**P1**–**P10**). The full representation of these structures is placed in Figures A1–A10.

Table 1. Investigated BODIPYs structures and experimental parameters (λ_{max} abs, λ_{max} em and Φ) from ref [50].

Compound	R_1	R_2	R_3	R_4	Solvent	λ_{max} abs (nm)	λ_{max} em (nm)	Φ
Hydrogen in Meso and α and β Substitution								
B1	H	H	H	H	EtOH	499	535	0.93
B2	H	H	H	Me	EtOH	507	520	0.81
B3	H	Me	H	Me	EtOH	505	516	0.80
B4	H	Me	Me	Me	EtOH	528	535	0.56
B5	H	Me	Et	Me	EtOH	517	546	0.70
Aromatic in Meso and α and β Substitution								
B6	Phenyl	H	H	H	CH_2Cl_2	500	527	0.03
B7	2,4,6-trimethylbenzene	H	H	H	CH_2Cl_2	501	521	0.84
B8	2,4,6-trimethylbenzene	Me	H	Me	AcOEt	500	508	0.92
B9	2,4,6-trimethylbenzene	Me	Et	Me	CH_2Cl_2	526	535	0.72
Substitution on Aromatic Position								
B10	2,4,6-trimethoxybenzene	Me	Et	Me	AcOEt	527	535	0.86
B11	2,6-didecyloxybenzene	Me	Et	Me	EtOH	522	536	0.82
B12	2,6-dichlorobenzene	Me	Et	Me	CH_2Cl_2	536	548	0.65
B13	1,3-di-tert-butylbenzene	Me	H	Me	CH_2Cl_2	499	507	0.97

Table 1. *Cont.*

Compound	R_1	R_2	R_3	R_4	Solvent	λ_{max} abs (nm)	λ_{max} em (nm)	Φ
Meso-Amino Derivatives								
B14	H	H	H	H	MeOH	497	507	0.87
B15	NH_2	H	H	H	MeOH	399	437	0.92
B16	NMe_2	H	H	H	MeOH	395	438	0.09
B17	Piperidine	H	H	H	MeOH	413	537	0.001
B18	*N*-aniline	H	H	H	MeOH	403	461	0.16
B19	*N*-phenylmethanamine	H	H	H	MeOH	403	453	0.09
Meso-alkoxy derivatives								
B20	H	H	H	H	Cy	504	511	0.96
B21	OMe	H	H	H	Cy	452	487	0.84
B22	OEt	H	H	H	Cy	451	487	0.96
B23	OPh	H	H	H	Cy	451	486	0.88
Others								
B24	4-iodobenzene	H	H	Ph	$CHCl_3$	555	588	0.20
B25	4-iodobenzene	H	H	1-napthalene	$CHCl_3$	542	607	0.38
B26	4-iodobenzene	H	H	PhOMe	$CHCl_3$	582	626	0.42
B27	4-iodobenzene	H	H	4-fluorobenzene	$CHCl_3$	555	590	0.22
B28	Phenyl	H	H	$CH{=}CH_2Ph$	CH_3CN	628	642	0.84
B29	-	Ph	H	Ph	$CHCl_3$	650	672	0.34
B30	-	PhOMe	H	Ph	$CHCl_3$	672	695	0.23

Me = Methyl, Et = Ethyl, AcOEt = Ethyl acetate, Ph = Phenyl, Cy = Cyclohexhane.

Table 2. Test group composed by related pyrrole-based dyes.

Compound	Solvent	λ_{max} abs (nm)	λ_{max} em (nm)	Φ	Ref
P1	CH_2Cl_2	442	465	0.95	[51]
P2	CH_2Cl_2	467	485	0.92	[51]
P3	CH_2Cl_2	453	497	1.00	[52]
P4	$CHCl_3$	508	524	0.96	[52]
P5	Toluene	419	649	0.11	[53,54]
P6	Toluene	633	783	0.28	[55]
P7	Benzene	693	698	0.43	[56]
P8	CH_2Cl_2	416	671	0.14	[53,54]
P9	DMSO	507	519	0.74	[57]
P10	DMSO	562	580	0.57	[57]

3. Results and Discussion

3.1. Optimisation of the BODIPYs Structures and Orbitals Parameters

Optimization processes were carried out with different functionals, respectively the one used for the TD-DFT calculation. No imaginary frequencies were observed for any of the investigated molecules nor for any functionals used assessing the correct energy minimization of the structure. Regarding structural features, most of the BODIPY core are planar or quasi planar with small deviation up to 30 degree in extreme cases. This issue has already been addressed by Orte and coworkers [27] and, in our case, did not explicitly interfere with the TD-DFT calculations for the estimation of the 0-0 transition.

The frontier molecular orbitals (HOMO (Highest Occupied Molecular Orbital) and LUMO (Lowest Unoccupied Molecular Orbital)) were generated and checked in order to verify that the correct modeling of the S_1 state was achieved. Figure 2 depicts the HOMO-LUMO levels and MO contours for **B1**, **B17,** and **B23**. The HOMO-LUMO gaps are in good

agreement with the BODIPY family standard values [50]. Generally, the HOMOs are built upon on the π-systems located on the pyrrole rings. Concurrently, the LUMOs are partially located on the meso-position accompanied by a depletion of the pyrrole π-systems relative to that found for the HOMOs. Minor contributions are also computed on the two fluorides of the BF_2 group. When bulky groups, aromatics or conjugated systems are present at the meso-position, the LUMOs tend to extend towards these groups directly linked or through a heteroatom (i.e., oxygen or nitrogen). This interaction could be described as an intramolecular partial charge transfer.

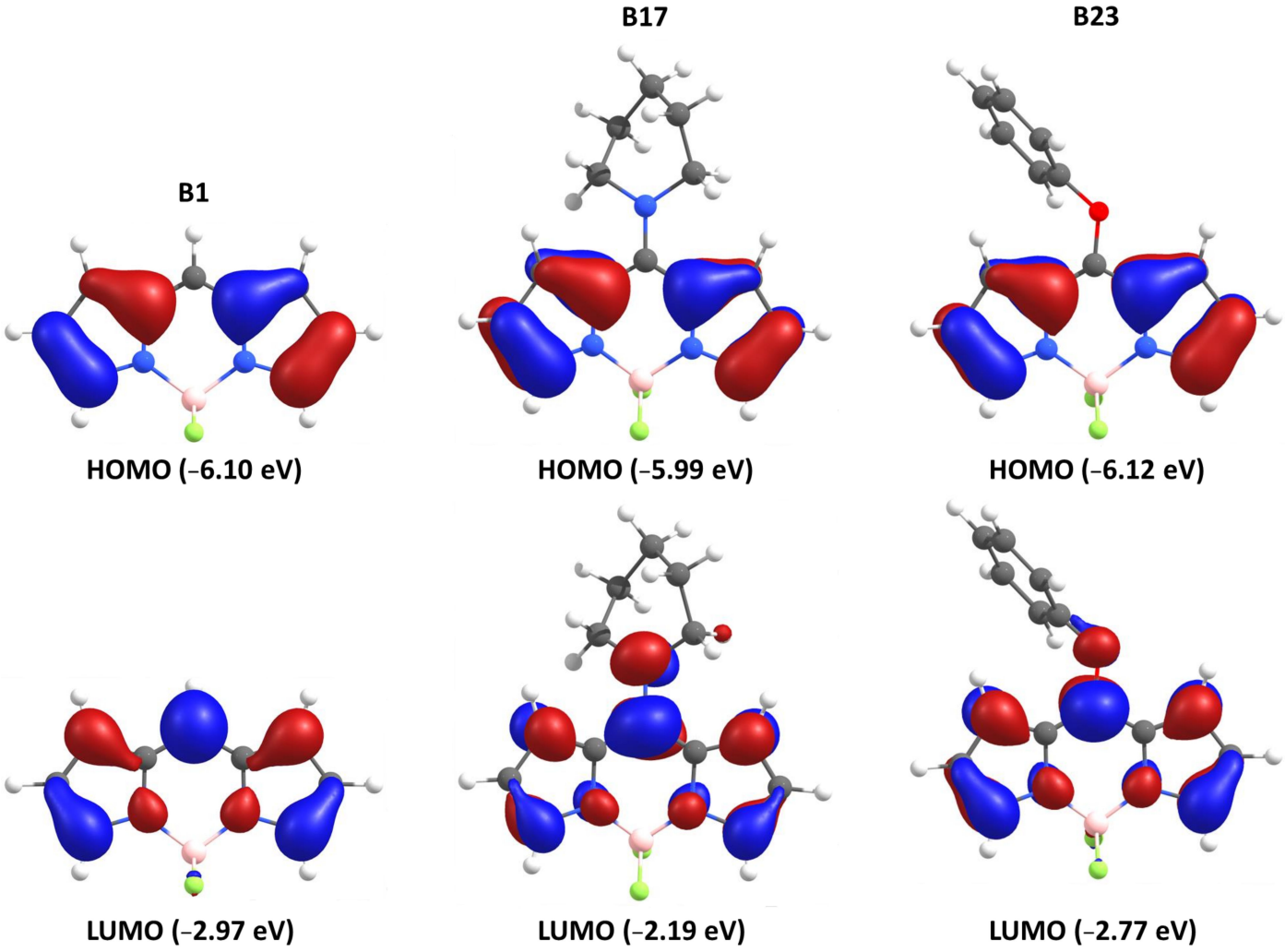

Figure 2. Comparison of the HOMO and LUMO contours for three selected investigated BODIPY's.

3.2. TD-DFT Assessing the First Excited State

The lowest energy spin-allowed electronic transitions calculated from TD-DFT computations have been correlated with the maximum 0-0 peak in the absorption experimental spectra. Figure 3 shows these correlations compared with the ideal case where these values are identical. The computed values are systematically lower than the experimental, which is consistent with the literature [35,36].

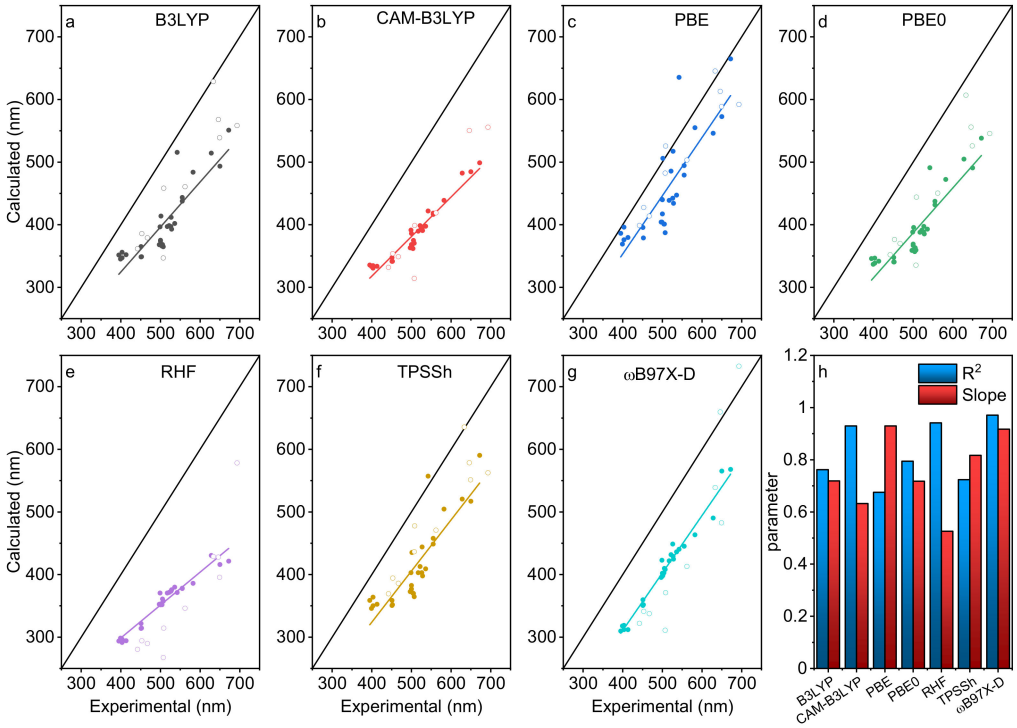

Figure 3. (**a**–**g**) graphs representing the calculated positions of the 0,0 $S_0 \rightarrow S_1$ absorption peaks against the experimental values for various DFT computational methods. The straight black line represents the cases where the experimental values are equal to the theoretical ones. The dark dots (●) are the training series (**B1–B30**) and the empty circles (○) are the test series (**P1–P10**). (**h**) linear regression parameters taken into consideration of the benchmarks. The experimental data are from Tables 1 and 2, and the appropriate solvent field has been applied.

To pin down what computational method appears the best, least square regressions have been performed on each dataset. Each of them consists of the lowest energy spin-allowed electronic transitions obtained from TD-DFT (as described in the computational details) and the positions of the maximum intensity peak (i.e., 0-0) in UV–vis spectra. Two parameters have been extracted: the R^2 correlation and the slope. A R^2 value approaching one implies a perfect or quasi-perfect correlation between computed and experimental wavelengths. Concurrently, a slope approaching one means that the deltas between each molecular species are the same numerical values. The "sensitivity" would be ideal in this case. Figure 3h displays these correlation parameters after a linear regression for each method for all 30 species. ωB97X-D seems to be the best suitable functional with the BODIPY dyes along with CAM-B3LYP as well as RHF methods.

Figure 4 regroups the correlation parameters R^2 separated by BODIPY groups as defined in "Investigated Structures" section. The CAM-B3LYP and ωB97X-D functionals as well as the RHF method appear to give results with good correlation with experiments (blue bars). The presence of an aromatic group (at the meso position in these series) has the greatest impact on the correlation mainly for the B3LYP, PBE, and PBE0. This, with the fact that ωB97X-D functional is giving the best results, indicates that the long-distance electronic correlation is important for this purpose. Indeed, this functional includes a 100% long-range exact exchange in its definition. For the investigated dyes, this interaction seems to be primordial during the interaction between light and a conjugated system and the formation of the charge transfer S_1 state. In comparison with a previous study on generic organic molecules, a more exact long-range term is needed (~25% vs. 100%) [58]. In the cases of the B3LYP, PBE, PBE0, and TPSSh and RHF methods, low R^2 values are obtained for molecules containing aromatic groups placed at the meso and α and β positions and substituents at various positions on the aromatic groups (**B10–B13**). However, an investigation as whether the inclusion or exclusion of specific groups on the BODIPY skeleton have any effect, has

been examined. However, this endeavor was inconclusive. Adding or removing dyes has a neglectable effect on the resulting fits (R^2 and slope) for each series. These tests have been performed by removing one dye at the time and examining what the effect on R^2 and slope are (Table A2).

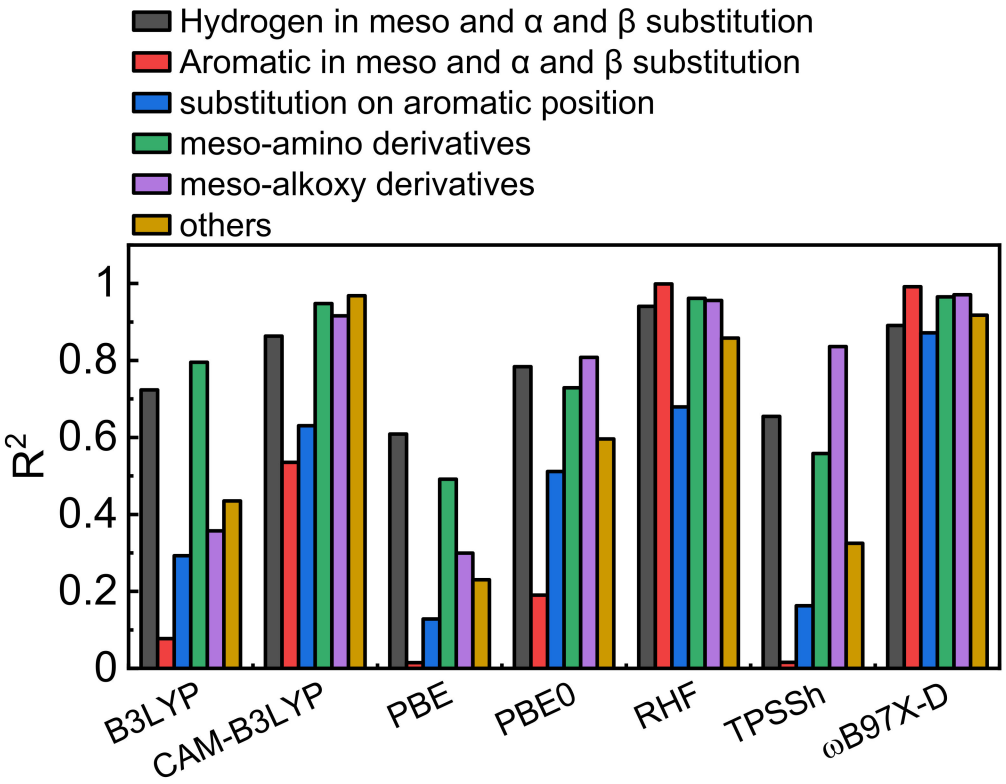

Figure 4. Correlation between R^2 and the computational method for each family of BODIPY derivatives. Dark grey: No substituent placed at the meso, α, and β positions. Red: Aromatic groups placed at the meso, α, and β positions. Blue: Various substitutions placed on the aromatics. Green: Amino groups placed at the meso position. Brown: Other cases.

3.3. Model Validation

In order to validate this computational model obtained with the training series (dark dots; (**B1**–**B30**), a test group (**P1**–**P10**) represented in Figure 3 by empty circles were added to the graphs. The test group is composed of analogous ring-fused and larger cyclic pyrrole-based dyes such as BOPHYs (bis(difluoroboron)1,2-bis((1H-pyrrol-2-yl)methylene)hydrazine (**P1**–**P4**)), free base porphyrinoides (tetraphenyl porphyrin **P5**, tetrabenzonporphyrin **P6**, phtalocyanine **P7,** and corrole **P8**) and diketo-pyrrolopyrroles (**P9**–**P10**) with common substituents to ensure a high degree of diversity. With little to no surprise, the best fits were again observed for the CAM-B3LYP and the ωB97X-D functionals as well as the RHF method. For B3LYP, PBE, and PBE0, the results are spread too widely to consider them as adequate functionals for this purpose.

3.4. The "Fudge Factor" Approach

Regarding the deviation of the slopes from the theoretical perfect theoretical match (black line in Figure 3), similarly to many other research groups, a "fudge factor" correction is also applied. This approach is generally accepted and is motivated on the ratio computation time vs quality of the method permitting to achieve a correlation slope close to 1 with a maximal R^2. Based on the large computational investigation above, ωB97X-D with 6.311g (d,p) basis set appear the most appropriate for the largest set of different substrates (Figure 4) and were selected to test the *fudge factor* (Figure 5). The calculated data set was plotted on Figure 5 with a R^2 of 0.97 and a slope of 0.917. After a mathematical correction of

the data set, a simple linear equation was established in order to achieve a reasonable precision and accuracy. This simple correction procedure is a common method used throughout the literature and allows to estimate absorption 0-0 peak position with quick and low cost calculations [18,38,49]. The resulting sought equation is placed inside Figure 5.

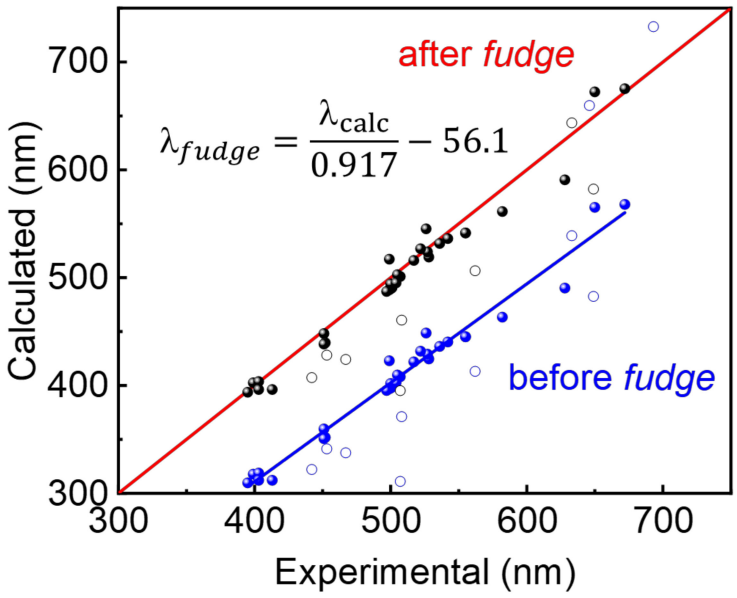

Figure 5. Linear correction obtained upon the use of the ωB97X-D with 6.311g (d,p) basis set.

4. Materials and Methods

The computations have been carried out with the Gaussian16 package [59] and ORCA 4.2.0 [60]. The calculations consisted in a simple three step-procedure. The geometries of all 30 BODIPYs and related pyrroliques dyes were preoptimized in their ground state with the B3LYP functional in conjunction with the 6-311g(d,p) basis set, as they are generally robust parameters for organic molecules in the literature. The optimized geometries were taken as starting points for optimization with solvent model (CPCM [61]) with each functional described below. Finally, TD-DFT computations were performed using the basis set 6-311g(d,p) in conjugation with def2-TZVP (Valence triple-zeta basis set) for heavy atoms. More precisely, B3LYP [62,63], CAM-B3LYP [64], PBE [65], PBE0 [66], TPSSh [67], and ωB97X-D [68] in addition of the RHF method [69] were used. Geometries were kept fixed during the TD-DFT computations and the excited state of interest (first excitation state, N = 1) was retrieved for each molecule. DFT integration grid was set to 4 and the final grid was set to 5. All other parameters were kept at their default values. Table A1 regroups all numerical data calculated for each method. The fudge correction was performed in two steps: first the calculated parameters were plotted against the experimental ones and fitted with a linear regression. Slope, R^2 and intercept were obtained. Second, the equation of the linear regression was then equalized with the x = y diagonal to obtain a translation equation.

5. Conclusions

An improved computational methodology for the prediction of the low-energy absorption peak of the BODIPY dyes has been developed. This method appears as a promising method with a lot of potential for applications because it is simple, cost effective and relatively accurate. As stated in the Introduction, many studies have addressed this important problem, but a good all-around method was not yet available. A wide benchmark series of TD-DFT methods, namely, to examine a large spread of possible wavelength values in the absorption spectra of a series of 30 BODIPYs, was employed and then validated with a test group of 10 related structures. The investigated BODIPYs included anchored groups such aromatics, electro-acceptor/donor substituents and saturated carbons chains to ensure

that the design methodology could be applied in a more general manner. The best results were obtained using the ωB97X-D functional (with the basis set 6-311g(d,p)) giving the best correlation parameters ($R^2 > 0.97$). Concurrently, this study also pointed out that the electronic correlation at long distance is important to describe the BODIPYs first excited state. However, in the classic situation for a need of anticipated absorption maximum of the $S_0 \rightarrow S_1$ transition for the BODIPY dyes, the "fudge factor" approach is a relatively affordable (i.e., best ratio accuracy vs computational resources) method (meaning relatively acceptable predicted values for relatively short computational time).

Author Contributions: Conceptualization, B.H., R.G. and P.D.H.; Data curation, A.S. (Adrien Schlachter), A.F., and K.T.; Formal analysis, A.S. (Adrien Schlachter) and A.F.; Funding acquisition, A.S. (Armand Soldera) and P.D.H.; Investigation, A.S. (Adrien Schlachter) and P.D.H.; Methodology, A.S. (Adrien Schlachter); Project administration, A.S. (Adrien Schlachter), A.S. (Armand Soldera), and P.D.H.; Resources, A.S. (Armand Soldera) and P.D.H.; Software, A.S. (Adrien Schlachter), A.F. and K.T.; Supervision, A.S. (Armand Soldera) and P.D.H.; Validation, A.S. (Adrien Schlachter), A.F. and P.D.H.; Visualization, A.S. (Adrien Schlachter); Writing—original draft, A.S. (Adrien Schlachter), A.F. and P.D.H.; Writing—review and editing, A.S. (Adrien Schlachter) and P.D.H. All authors have read and agreed to the published version of the manuscript.

Funding: This research was funded by the Natural Sciences and Engineering Research Council of Canada (NSERC). The computational resources were provided by Calcul Québec and Compute Canada.

Institutional Review Board Statement: Not applicable.

Informed Consent Statement: Not applicable.

Data Availability Statement: The data presented in this study are available upon request.

Acknowledgments: The authors wish to thank Alexandra Guilbault for additional calculations.

Conflicts of Interest: The authors declare no conflict of interest.

Sample Availability: Not available.

Appendix A

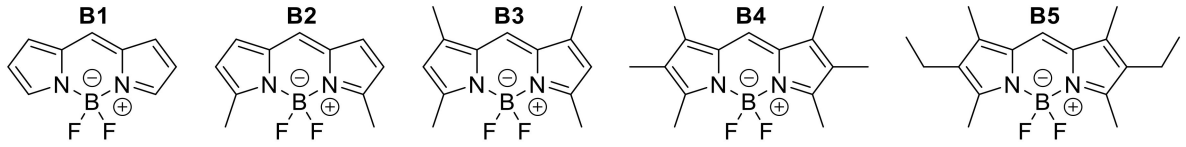

Figure A1. Hydrogen atoms placed at the meso position.

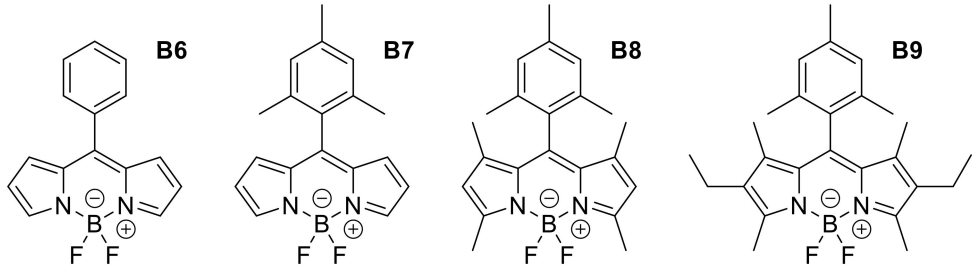

Figure A2. Aromatic groups placed at the meso position.

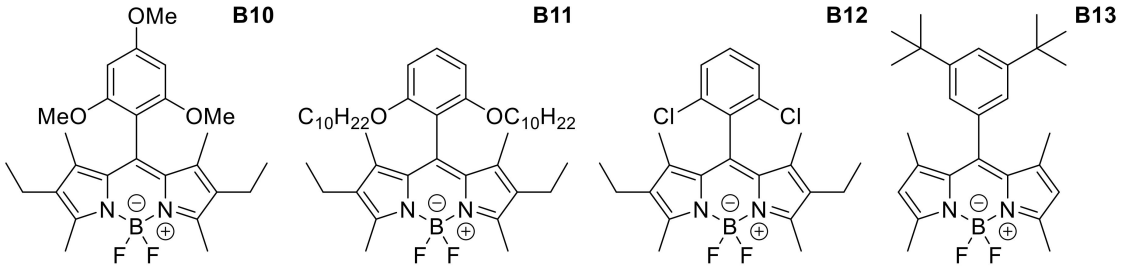

Figure A3. Substituted aromatic groups placed at the meso position.

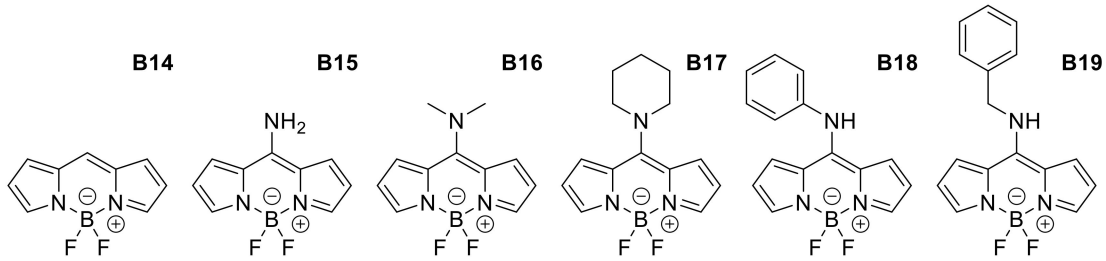

Figure A4. Amino groups placed at the meso position.

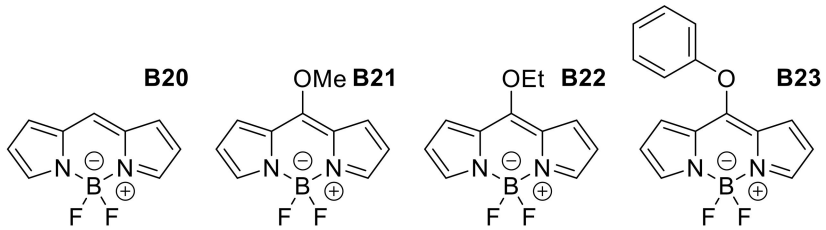

Figure A5. Alkoxy groups placed at the meso position.

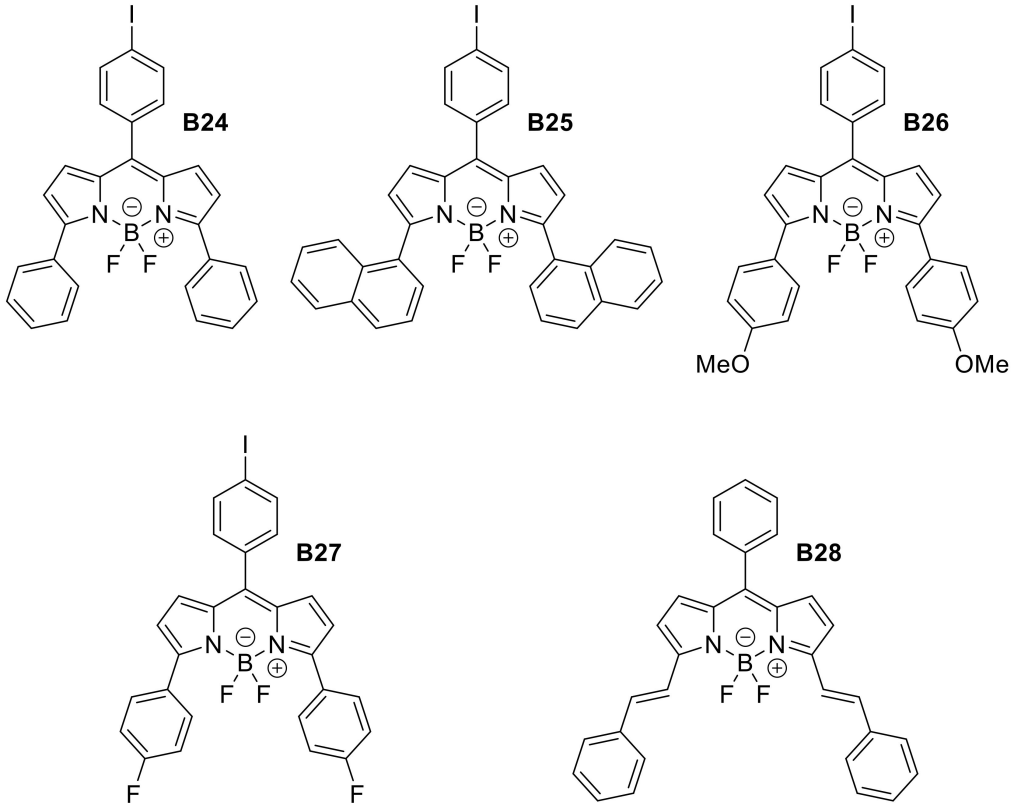

Figure A6. Aromatic groups placed at the meso and α positions.

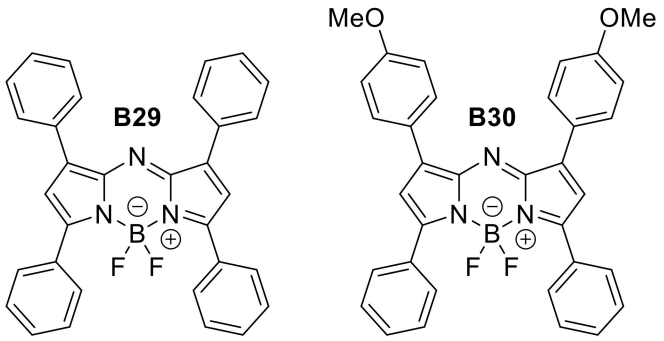

Figure A7. azaBODIPY with substituents at α and β positions.

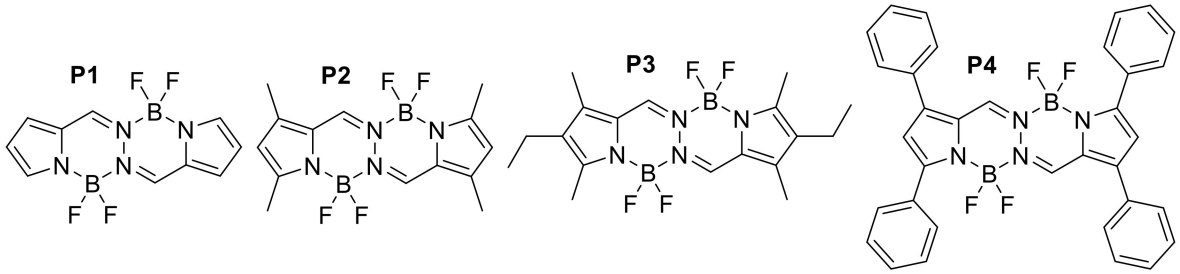

Figure A8. Various BOPHYs.

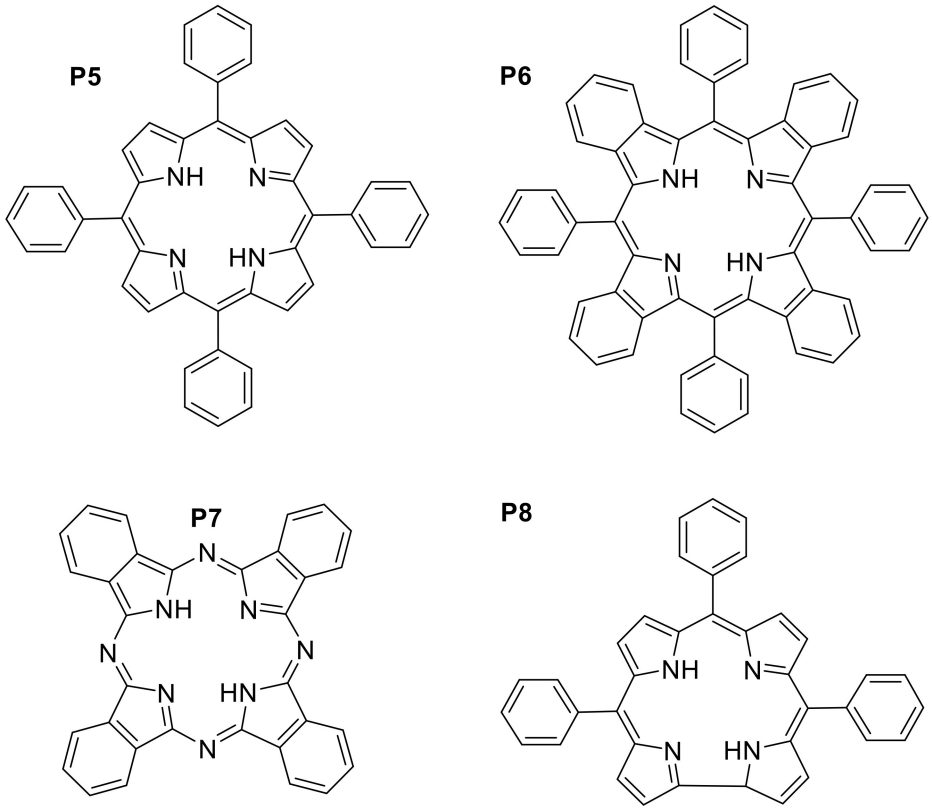

Figure A9. Porphyrinoides.

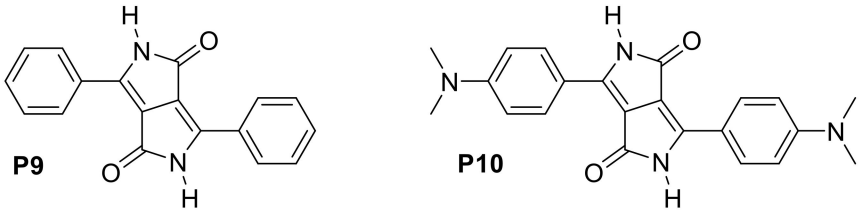

Figure A10. Diketo-pyrrolopyrroles.

Appendix B

Table A1. Comparison of the experimental position of the 0-0 peak of the low-energy absorption band with the calculated ones for all investigated structures.

Compound	λ_{max} abs (nm)	B3LYP	CAM-B3LYP	PBE	PBE0	RHF	TPSSh	ωB97X-D	ωB97X-D fudge
B1	499	368	363.1	404.2	358.9	352.5	372.9	396.9	488.81
B2	507	364.9	370.4	387.3	359.5	357.5	364.6	408.12	501.05
B3	505	368.3	375	400.9	363.1	360.9	369.7	409.75	502.82
B4	528	393	390.8	434.2	385.3	375.7	397.7	424.65	519.07
B5	517	397.1	389.8	438.8	388	370.6	403	421.87	516.04
B6	500	375.3	368.2	417.3	366.9	351.9	382.5	397.65	489.63
B7	501	413.9	366.8	506	395.5	353.4	435.3	398.58	490.65
B8	500	374	385.9	439.9	369	351.8	377	401.89	494.25
B9	526	397	393.1	442.4	388.6	373.2	403	448.72	545.31
B10	527	411.8	394.9	517.4	397.4	373.9	444	429.12	523.94
B11	522	398.6	398.6	485.7	391.2	371.6	412.8	431.8	526.86
B12	536	401.9	397.5	447.3	393	379.9	409.2	436.21	531.67
B13	499	396.6	391.3	440.6	388.2	370.4	403	422.89	517.15
B14	497	368.1	363.2	404.2	359	352.6	372.8	395.37	487.15
B15	399	345.1	333.3	369	336.7	298.4	345.9	317.78	402.56
B16	395	351.6	335.5	386.2	345.8	293.9	358.8	309.67	393.72
B17	413	352	333.6	379.7	341.7	294.3	352.5	312.05	396.31
B18	403	355.9	334.6	396	346.7	296.7	363.8	318.81	403.68
B19	403	347.2	330.7	375.9	338.5	291.5	350.2	312.05	396.31
B20	504	365.8	362	400.9	357.1	351.7	370.3	402.67	495.11
B21	452	348.9	341.6	378.8	340.6	314.5	351.7	351.78	439.63
B22	451	348.7	341.5	395.7	340.5	313.9	350.5	350.67	438.42
B23	451	365	347.3	395.7	347.7	321.8	358.7	359.66	448.22
B24	555	437.6	416.5	479.2	431.7	378.2	448.6	445.17	541.44
B25	542	515.5	421.9	635.3	491.1	371.3	557.3	440.39	536.23
B26	582	483.9	438.8	554.9	472.4	385.9	504.6	463.41	561.32
B27	555	443.5	418.5	494.5	437.5	377.6	457.7	445.2	541.47
B28	628	514.3	482.3	546.1	504.7	430.4	520.5	490.36	590.70
B29	650	493.5	484.7	572.7	490.7	416	517	565.21	672.30
B30	664	551	498.9	664.8	538.3	421.3	590.5	567.93	675.27
P1	442	361.6	332	398.7	352	280.4	369.2	322.12	407.29
P2	467	379	348.8	413.8	370.1	289.9	385.9	337.65	424.22
P3	453	385.7	353.8	427.6	376.4	294.2	394.3	341.29	428.19
P4	508	458.2	398.8	525.6	444	314.5	477.7	371.07	460.66
P5	646	567.9	550.6	613	556	427.8	578.7	659.64	775.25
P6	633	628.8	-	645.4	606.9	428.9	635.7	538.87	643.59
P7	693	558.3	555.6	592.2	545.6	578.4	562.6	732.8	855.01
P8	649	538.9	-	588.6	525.9	395.5	551.2	482.58	582.22
P9	507	346.8	314.1	482.4	335.4	267.5	436.5	311.06	395.23
P10	562	460.7	419	503.2	450.4	346.1	470.8	413.11	506.49

Appendix C

Table A2. Variation of the parameters R^2 and slope when adding or removing one dye at the time from the training data set for each computational method.

Removed Dye	B3LYP		CAM-B3LYP		PBE		PBE0		RHF		TPSSh		ωB97X-D	
	Slope	R^2	Slope	R^2	Slope	R^2	Slope	R^2	Slope	R^2	Slope	R^2	Slope	R^2
None	0.72	0.76	0.63	0.93	0.93	0.68	0.72	0.79	0.53	0.94	0.82	0.72	0.92	0.97
B1	0.72	0.77	0.63	0.93	0.93	0.68	0.72	0.80	0.53	0.94	0.81	0.73	0.92	0.97
B2	0.72	0.77	0.63	0.93	0.93	0.69	0.72	0.80	0.53	0.94	0.82	0.74	0.92	0.97
B3	0.72	0.77	0.63	0.93	0.93	0.69	0.72	0.80	0.53	0.94	0.82	0.73	0.92	0.97
B4	0.72	0.77	0.63	0.93	0.94	0.68	0.72	0.80	0.52	0.94	0.82	0.73	0.92	0.97
B5	0.72	0.76	0.63	0.93	0.93	0.68	0.72	0.80	0.52	0.94	0.82	0.73	0.92	0.97
B6	0.72	0.77	0.63	0.93	0.93	0.68	0.72	0.80	0.53	0.94	0.82	0.73	0.92	0.97
B7	0.72	0.76	0.63	0.93	0.93	0.69	0.72	0.79	0.53	0.94	0.82	0.73	0.92	0.97
B8	0.72	0.77	0.63	0.93	0.93	0.68	0.72	0.80	0.53	0.94	0.82	0.73	0.92	0.97
B9	0.72	0.77	0.63	0.93	0.93	0.68	0.72	0.80	0.52	0.94	0.82	0.73	0.91	0.98
B10	0.72	0.76	0.63	0.93	0.92	0.68	0.72	0.79	0.52	0.94	0.81	0.72	0.92	0.97
B11	0.72	0.76	0.63	0.93	0.93	0.68	0.72	0.80	0.52	0.94	0.82	0.72	0.92	0.97
B12	0.72	0.77	0.63	0.93	0.94	0.68	0.72	0.80	0.52	0.94	0.82	0.73	0.92	0.97
B13	0.72	0.76	0.63	0.93	0.93	0.67	0.72	0.79	0.53	0.95	0.82	0.72	0.92	0.98
B14	0.72	0.77	0.63	0.93	0.93	0.68	0.72	0.80	0.53	0.94	0.81	0.73	0.92	0.97
B15	0.74	0.76	0.65	0.93	0.94	0.66	0.74	0.79	0.53	0.94	0.84	0.72	0.92	0.97
B16	0.75	0.77	0.65	0.94	0.96	0.68	0.75	0.80	0.52	0.94	0.85	0.73	0.92	0.97
B17	0.73	0.76	0.64	0.93	0.94	0.67	0.73	0.79	0.52	0.94	0.83	0.72	0.91	0.97
B18	0.74	0.77	0.64	0.93	0.96	0.68	0.74	0.80	0.52	0.94	0.85	0.73	0.92	0.97
B19	0.74	0.76	0.64	0.93	0.95	0.67	0.74	0.79	0.52	0.94	0.84	0.72	0.92	0.97
B20	0.72	0.77	0.63	0.94	0.93	0.68	0.72	0.80	0.53	0.94	0.82	0.73	0.92	0.97
B21	0.71	0.76	0.63	0.93	0.92	0.67	0.71	0.79	0.52	0.94	0.81	0.72	0.91	0.97
B22	0.71	0.76	0.63	0.93	0.93	0.67	0.71	0.79	0.52	0.94	0.81	0.72	0.91	0.97
B23	0.72	0.76	0.63	0.93	0.93	0.67	0.72	0.79	0.52	0.94	0.81	0.72	0.92	0.97
B24	0.72	0.76	0.63	0.93	0.94	0.68	0.72	0.79	0.53	0.94	0.82	0.72	0.92	0.97
B25	0.70	0.83	0.63	0.93	0.89	0.77	0.70	0.84	0.53	0.94	0.79	0.81	0.92	0.97
B26	0.70	0.75	0.63	0.93	0.91	0.66	0.70	0.79	0.53	0.94	0.80	0.71	0.93	0.97
B27	0.72	0.76	0.63	0.93	0.93	0.67	0.71	0.79	0.53	0.94	0.81	0.72	0.92	0.97
B28	0.69	0.73	0.61	0.93	0.95	0.66	0.69	0.77	0.51	0.94	0.81	0.70	0.95	0.98
B29	0.73	0.74	0.62	0.92	0.95	0.65	0.72	0.77	0.54	0.94	0.83	0.70	0.89	0.97
B30	0.67	0.70	0.62	0.91	0.84	0.59	0.68	0.74	0.56	0.95	0.75	0.65	0.91	0.96

References

1. Chen, D.; Zhong, Z.; Ma, Q.; Shao, J.; Huang, W.; Dong, X.; Dong, X. Aza-BODIPY-Based Nanomedicines in Cancer Phototheranostics. *ACS Appl. Mater. Interfaces* **2020**, *12*, 26914–26925. [CrossRef]
2. Liu, M.; Li, C. Recent Advances in Activatable Organic Photosensitizers for Specific Photodynamic Therapy. *Chempluschem* **2020**, *85*, 948–957. [CrossRef]
3. Poddar, M.; Misra, R. Recent advances of BODIPY based derivatives for optoelectronic applications. *Coord. Chem. Rev.* **2020**, *421*, 213462. [CrossRef]
4. Klfout, H.; Stewart, A.; Elkhalifa, M.; He, H. BODIPYs for Dye-Sensitized Solar Cells. *ACS Appl. Mater. Interfaces* **2017**, *9*, 39873–39889. [CrossRef]
5. Ho, D.; Ozdemir, R.; Kim, H.; Earmme, T.; Usta, H.; Kim, C. BODIPY-Based Semiconducting Materials for Organic Bulk Heterojunction Photovoltaics and Thin-Film Transistors. *Chempluschem* **2018**, *84*, cplu.201800543. [CrossRef]
6. Bessette, A.; Hanan, G.S. Design, synthesis and photophysical studies of dipyrromethene-based materials: Insights into their applications in organic photovoltaic devices. *Chem. Soc. Rev.* **2014**, *43*, 3342–3405. [CrossRef] [PubMed]
7. Squeo, B.M.; Pasini, M. BODIPY platform: A tunable tool for green to NIR OLEDs. *Supramol. Chem.* **2020**, *32*, 56–70. [CrossRef]
8. Chiba, Y.; Nakamura, T.; Matsuoka, R.; Nabeshima, T. Synthesis and Functions of Oligomeric and Multidentate Dipyrrin Derivatives and their Complexes. *Synlett* **2020**, *31*, 1663–1681. [CrossRef]
9. Praveen, V.K.; Vedhanarayanan, B.; Mal, A.; Mishra, R.K.; Ajayaghosh, A. Self-Assembled Extended π-Systems for Sensing and Security Applications. *Acc. Chem. Res.* **2020**, *53*, 507. [CrossRef]
10. Liu, Z.; Jiang, Z.; Yan, M.; Wang, X. Recent Progress of BODIPY Dyes with Aggregation-Induced Emission. *Front. Chem.* **2019**, *7*, 712. [CrossRef] [PubMed]

11. Toliautas, S.; Dodonova, J.; Žvirblis, A.; Čiplys, I.; Polita, A.; Devižis, A.; Tumkevičius, S.; Šulskus, J.; Vyšniauskas, A. Enhancing the Viscosity-Sensitive Range of a BODIPY Molecular Rotor by Two Orders of Magnitude. *Chem. A Eur. J.* **2019**, *25*, 10342–10349. [CrossRef] [PubMed]
12. Lin, Z.; Kohn, A.W.; Van Voorhis, T. Toward Prediction of Nonradiative Decay Pathways in Organic Compounds II: Two Internal Conversion Channels in BODIPYs. *J. Phys. Chem. C* **2020**, *124*, 3925–3938. [CrossRef]
13. Ou, Q.; Peng, Q.; Shuai, Z. Toward Quantitative Prediction of Fluorescence Quantum Efficiency by Combining Direct Vibrational Conversion and Surface Crossing: BODIPYs as an Example. *J. Phys. Chem. Lett.* **2020**, *11*, 7790–7797. [CrossRef]
14. López Arbeloa, F.; Bañuelos, J.; Martínez, V.; Arbeloa, T.; López Arbeloa, I. Structural, photophysical and lasing properties of pyrromethene dyes. *Int. Rev. Phys. Chem.* **2005**, *24*, 339–374. [CrossRef]
15. Wei, Y.; Zheng, M.; Zhou, Q.; Zhou, X.; Liu, S. Application of a bodipy-C70 dyad in triplet-triplet annihilation upconversion of perylene as a metal-free photosensitizer. *Org. Biomol. Chem.* **2018**, *16*, 5598–5608. [CrossRef]
16. Spiegel, J.D.; Lyskov, I.; Kleinschmidt, M.; Marian, C.M. Charge-transfer contributions to the excitonic coupling matrix element in BODIPY-based energy transfer cassettes. *Chem. Phys.* **2017**, *482*, 265–276. [CrossRef]
17. Thorat, K.G.; Kamble, P.; Ray, A.K.; Sekar, N. Novel pyrromethene dyes with N-ethyl carbazole at the meso position: A comprehensive photophysical, lasing, photostability and TD-DFT study. *Phys. Chem. Chem. Phys.* **2015**, *17*, 17221–17236. [CrossRef]
18. Thorat, K.G.; Kamble, P.; Mallah, R.; Ray, A.K.; Sekar, N. Congeners of Pyrromethene-567 Dye: Perspectives from Synthesis, Photophysics, Photostability, Laser, and TD-DFT Theory. *J. Org. Chem.* **2015**, *80*, 6152–6164. [CrossRef] [PubMed]
19. Ünal, H.; Gunceler, D.; Mete, E. A study of the density functional methods on the photoabsorption of Bodipy dyes. *J. Photochem. Photobiol. A Chem.* **2014**, *278*, 14–18. [CrossRef]
20. Shandura, M.P.; Yakubovskyi, V.P.; Gerasov, A.O.; Kachkovsky, O.D.; Poronik, Y.M.; Kovtun, Y.P. α-Polymethine-Substituted Boron Dipyrromethenes—BODIPY-Based NIR Cyanine-Like Dyes. *Eur. J. Org. Chem.* **2012**, *2012*, 1825–1834. [CrossRef]
21. Irmler, P.; Winter, R.F. σ-Pt-BODIPY Complexes with Platinum Attachment to Carbon Atoms C2 or C3: Spectroscopic, Structural, and (Spectro)Electrochemical Studies and Photocatalysis. *Organometallics* **2018**, *37*, 235–253. [CrossRef]
22. Dong, Y.; Iagatti, A.; Foggi, P.; Zhao, J.; Mazzone, G.; Xu, K.; Ji, W.; Di Donato, M.; Russo, N. Bodipy-squaraine triads: Preparation and study of the intramolecular energy transfer, charge separation and intersystem crossing. *Dye. Pigment.* **2017**, *147*, 560–572. [CrossRef]
23. Shi, W.-J.; Kinoshita, T.; Ng, D.K.P. Ethynyl-Linked Donor-π-Acceptor Boron Dipyrromethenes for Panchromatic Dye-Sensitized Solar Cells. *Asian J. Org. Chem.* **2017**, *6*, 758–767. [CrossRef]
24. Chong, H.; Fron, E.; Liu, Z.; Boodts, S.; Thomas, J.; Harvey, J.N.; Hofkens, J.; Dehaen, W.; Van der Auweraer, M.; Smet, M. Acid-Sensitive BODIPY Dyes: Synthesis through Pd-Catalyzed Direct C(sp^3)−H Arylation and Photophysics. *Chem. A Eur. J.* **2017**, *23*, 4687–4699. [CrossRef]
25. Misra, R. Tuning of Second-Order Nonlinear Optical Response Properties of Aryl-Substituted Boron-Dipyrromethene Dyes: Unidirectional Charge Transfer Coupled with Structural Tailoring. *J. Phys. Chem. C* **2017**, *121*, 5731–5739. [CrossRef]
26. Mao, M.; Li, Q.S.; Zhang, X.L.; Wu, G.H.; Dai, C.G.; Ding, Y.; Dai, S.Y.; Song, Q.H. Effects of donors of bodipy dyes on the performance of dye-sensitized solar cells. *Dye. Pigment.* **2017**, *141*, 148–160. [CrossRef]
27. Orte, A.; Debroye, E.; Ruedas-Rama, M.J.; Garcia-Fernandez, E.; Robinson, D.; Crovetto, L.; Talavera, E.M.; Alvarez-Pez, J.M.; Leen, V.; Verbelen, B.; et al. Effect of the substitution position (2, 3 or 8) on the spectroscopic and photophysical properties of BODIPY dyes with a phenyl, styryl or phenylethynyl group. *RSC Adv.* **2016**, *6*, 102899–102913. [CrossRef]
28. Zinna, F.; Bruhn, T.; Guido, C.A.; Ahrens, J.; Bröring, M.; Di Bari, L.; Pescitelli, G. Circularly Polarized Luminescence from Axially Chiral BODIPY DYEmers: An Experimental and Computational Study. *Chem. A Eur. J.* **2016**, *22*, 16089–16098. [CrossRef] [PubMed]
29. Balsukuri, N.; Lone, M.Y.; Jha, P.C.; Mori, S.; Gupta, I. Synthesis, Structure, and Optical Studies of Donor-Acceptor-Type Near-Infrared (NIR) Aza-Boron-Dipyrromethene (BODIPY) Dyes. *Chem. Asian J.* **2016**, *11*, 1572–1587. [CrossRef]
30. De Vetta, M.; Corral, I. Insight into the optical properties of meso-pentafluorophenyl(PFP)-BODIPY: An attractive platform for functionalization of BODIPY dyes. *Comput. Theor. Chem.* **2019**, *1150*, 110–120. [CrossRef]
31. Ghosh, N.N.; Habib, M.; Pramanik, A.; Sarkar, P.; Pal, S. Tuning the BODIPY core for its potential use in DSSC: A quantum chemical approach. *Bull. Mater. Sci.* **2018**, *41*, 1–10. [CrossRef]
32. Pirillo, J.; Mazzone, G.; Russo, N. Theoretical Insights into the Switching Off/On of $^1O_2$ Photosensitization in Chemicontrolled Photodynamic Therapy. *Chem. A Eur. J.* **2018**, *24*, 3512–3519. [CrossRef] [PubMed]
33. Mazzone, G.; Quartarolo, A.D.; Russo, N. PDT-correlated photophysical properties of thienopyrrole BODIPY derivatives. Theoretical insights. *Dye. Pigment.* **2016**, *130*, 9–15. [CrossRef]
34. Le Guennic, B.; Jacquemin, D. Taking Up the Cyanine Challenge with Quantum Tools. *Acc. Chem. Res.* **2015**, *48*, 530–537. [CrossRef] [PubMed]
35. Charaf-Eddin, A.; Le Guennic, B.; Jacquemin, D. Excited-states of BODIPY–cyanines: Ultimate TD-DFT challenges? *RSC Adv.* **2014**, *4*, 49449–49456. [CrossRef]
36. Laurent, A.D.; Adamo, C.; Jacquemin, D. Dye chemistry with time-dependent density functional theory. *Phys. Chem. Chem. Phys.* **2014**, *16*, 14334–14356. [CrossRef] [PubMed]

37. Egidi, F.; Trani, F.; Ballone, P.A.; Barone, V.; Andreoni, W. Low-lying electronic excitations of a water-soluble BODIPY: From the gas phase to the solvated molecule. *Theor. Chem. Acc.* **2016**, *135*, 264. [CrossRef]
38. Rose, A.; Kumar, S.V.; Swavey, S.; Erb, J. A simple and efficient protocol for screening boron-dipyrromethene dyes using TD-DFT and an examination of the aryl-meso position. *Comput. Theor. Chem.* **2017**, *1118*, 107–114. [CrossRef]
39. Momeni, M.R.; Brown, A. Why do TD-DFT excitation energies of BODIPY/aza-BODIPY families largely deviate from experiment? Answers from electron correlated and multireference methods. *J. Chem. Theory Comput.* **2015**, *11*, 2619–2632. [CrossRef] [PubMed]
40. Chibani, S.; Laurent, A.D.; Le Guennic, B.; Jacquemin, D. Improving the accuracy of excited-state simulations of BODIPY and Aza-BODIPY dyes with a joint SOS-CIS(D) and TD-DFT approach. *J. Chem. Theory Comput.* **2014**, *10*, 4574–4582. [CrossRef] [PubMed]
41. Asaoka, M.; Kitagawa, Y.; Teramoto, R.; Miyagi, K.; Natori, Y.; Nakano, M. Origin of Solvent-independent Optical Property of Unsubstituted BODIPY Revisited. *Chem. Lett.* **2017**, *46*, 536–538. [CrossRef]
42. Chibani, S.; Jacquemin, D.; Laurent, A.D. Modelling solvent effects on the absorption and emission spectra of constrained cyanines with both implicit and explicit QM/EFP models. *Comput. Theor. Chem.* **2014**, *1040–1041*, 321–327. [CrossRef]
43. Filarowski, A.; Lopatkova, M.; Lipkowski, P.; Van Der Auweraer, M.; Leen, V.; Dehaen, W. Solvatochromism of BODIPY-Schiff dye. *J. Phys. Chem. B* **2015**, *119*, 2576–2584. [CrossRef] [PubMed]
44. Momeni, M.R.; Brown, A. A Local CC2 and TDA-DFT Double Hybrid Study on BODIPY/aza-BODIPY Dimers as Heavy Atom Free Triplet Photosensitizers for Photodynamic Therapy Applications. *J. Phys. Chem. A* **2016**, *120*, 2550–2560. [CrossRef]
45. Laurent, A.D.; Blondel, A.; Jacquemin, D. Choosing an atomic basis set for TD-DFT, SOPPA, ADC(2), CIS(D), CC2 and EOM-CCSD calculations of low-lying excited states of organic dyes. *Theor. Chem. Acc.* **2015**, *134*, 76. [CrossRef]
46. Briggs, E.A.; Besley, N.A.; Robinson, D. QM/MM excited state molecular dynamics and fluorescence spectroscopy of BODIPY. *J. Phys. Chem. A* **2013**, *117*, 2644–2650. [CrossRef]
47. Gawale, Y.; Sekar, N. Investigating the excited state optical properties and origin of large stokes shift in Benz[c,d]indole N-Heteroarene BF2 dyes with ab initio tools. *J. Photochem. Photobiol. B Biol.* **2018**, *178*, 472–480. [CrossRef]
48. Chibani, S.; Le Guennic, B.; Charaf-Eddin, A.; Laurent, A.D.; Jacquemin, D. Revisiting the optical signatures of BODIPY with ab initio tools. *Chem. Sci.* **2013**, *4*, 1950–1963. [CrossRef]
49. Machado, L.A.; de Souza, M.C.; da Silva, C.M.; Yoneda, J.; de Rezende, L.C.D.; Emery, F.S.; de Simone, C.A.; da Silva Júnior, E.N.; Pedrosa, L.F. On the synthesis, optical and computational studies of novel BODIPY-based phosphoramidate fluorescent dyes. *J. Fluor. Chem.* **2019**, *220*, 9–15. [CrossRef]
50. Loudet, A.; Burgess, K. BODIPY dyes and their derivatives: Syntheses and spectroscopic properties. *Chem. Rev.* **2007**, *107*, 4891–4932. [CrossRef] [PubMed]
51. Tamgho, I.-S.; Hasheminasab, A.; Engle, J.T.; Nemykin, V.N.; Ziegler, C.J. A New Highly Fluorescent and Symmetric Pyrrole–BF 2 Chromophore: BOPHY. *J. Am. Chem. Soc.* **2014**, *136*, 5623–5626. [CrossRef] [PubMed]
52. Boodts, S.; Fron, E.; Hofkens, J.; Dehaen, W. The BOPHY fluorophore with double boron chelation: Synthesis and spectroscopy. *Coord. Chem. Rev.* **2018**, *371*, 1–10. [CrossRef]
53. Taniguchi, M.; Du, H.; Lindsey, J.S. PhotochemCAD 3: Diverse Modules for Photophysical Calculations with Multiple Spectral Databases. *Photochem. Photobiol.* **2018**, *94*, 277–289. [CrossRef] [PubMed]
54. Taniguchi, M.; Lindsey, J.S. Database of Absorption and Fluorescence Spectra of >300 Common Compounds for use in PhotochemCAD. *Photochem. Photobiol.* **2018**, *94*, 290–327. [CrossRef]
55. Cui, X.; Zhao, J.; Yang, P.; Sun, J. Zinc(ii) tetraphenyltetrabenzoporphyrin complex as triplet photosensitizer for triplet-triplet annihilation upconversion. *Chem. Commun.* **2013**, *49*, 10221–10223. [CrossRef] [PubMed]
56. Freyer, W.; Mueller, S.; Teuchner, K. Photophysical properties of benzoannelated metal-free phthalocyanines. *J. Photochem. Photobiol. A Chem.* **2004**, *163*, 231–240. [CrossRef]
57. Vala, M.; Vyňuchal, J.; Toman, P.; Weiter, M.; Luňák, S. Novel, soluble diphenyl-diketo-pyrrolopyrroles: Experimental and theoretical study. *Dye. Pigment.* **2010**, *84*, 176–182. [CrossRef]
58. Jacquemin, D.; Wathelet, V.; Perpète, E.A.; Adamo, C. Extensive TD-DFT benchmark: Singlet-excited states of organic molecules. *J. Chem. Theory Comput.* **2009**, *5*, 2420–2435. [CrossRef] [PubMed]
59. Frisch, M.J.; Trucks, G.W.; Schlegel, H.B.; Scuseria, G.E.; Robb, M.A.; Cheeseman, J.R.; Scalmani, G.; Barone, V.; Petersson, G.A.; Nakatsuji, H.; et al. *Gaussian 16*; Revision B.01; Gaussian Inc.: Wallingford, CT, USA, 2016.
60. Hočevar, T.; Demčar, J. Computation of Graphlet Orbits for Nodes and Edges in Sparse Graphs. *J. Stat. Softw.* **2016**, *71*. [CrossRef]
61. Barone, V.; Cossi, M. Quantum calculation of molecular energies and energy gradients in solution by a conductor solvent model. *J. Phys. Chem. A* **1998**, *102*, 1995–2001. [CrossRef]
62. Adamo, C.; Barone, V. Toward reliable adiabatic connection models free from adjustable parameters. *Chem. Phys. Lett.* **1997**, *274*, 242–250. [CrossRef]
63. Becke, A.D. A new mixing of Hartree-Fock and local density-functional theories. *J. Chem. Phys.* **1993**, *98*, 1372–1377. [CrossRef]
64. Yanai, T.; Tew, D.P.; Handy, N.C. A new hybrid exchange-correlation functional using the Coulomb-attenuating method (CAM-B3LYP). *Chem. Phys. Lett.* **2004**, *393*, 51–57. [CrossRef]
65. Perdew, J.P.; Burke, K.; Ernzerhof, M. Generalized gradient approximation made simple. *Phys. Rev. Lett.* **1996**, *77*, 3865–3868. [CrossRef]

66. Adamo, C.; Barone, V. Toward reliable density functional methods without adjustable parameters: The PBE0 model. *J. Chem. Phys.* **1999**, *110*, 6158–6170. [CrossRef]
67. Tao, J.; Perdew, J.P.; Staroverov, V.N.; Scuseria, G.E. Climbing the density functional ladder: Nonempirical meta–generalized gradient approximation designed for molecules and solids. *Phys. Rev. Lett.* **2003**, *91*, 146401. [CrossRef] [PubMed]
68. Chai, J.D.; Head-Gordon, M. Long-range corrected hybrid density functionals with damped atom-atom dispersion corrections. *Phys. Chem. Chem. Phys.* **2008**, *10*, 6615–6620. [CrossRef] [PubMed]
69. Wheeler, S.E.; Allen, W.D.; Schaefer, H.F. On the convergence of *Z*-averaged perturbation theory. *J. Chem. Phys.* **2008**, *128*, 074107. [CrossRef] [PubMed]